INVERTIBLE MAPPING BETWEEN FIELDS IN CAMELS

Anonymous authors
Paper under double-blind review

ABSTRACT

We build a bijective mapping between different fields from IllustrisTNG in CAMELS Project. In this work, we train a CycleGAN on three different setups: translating dark matter to neutral hydrogen (Mcdm-HI), mapping between dark matter and magnetic fields magnitude (Mcdm-B), and finally predicting magnetic fields magnitude from neutral hydrogen (HI-B). We assess the performance of the models using various metrics such a probability distribution function (PDF) of the pixel values and 2D power spectrum ($P(k)$). Results suggest that in all setups, the model is capable of predicting the target field from the source field and vice versa, and the predicted maps exhibit statistical properties which are consistent with those of the target maps. This is indicated by the fact that the mean and standard deviation of the PDF of maps from the test set are in good agreement with those of the generated maps. The mean and variance of $P(k)$ of the real maps agree well with those of fake ones. The consistency tests on the model suggest that the source field can be recovered reasonably well by a forward mapping (source to target) followed by a backward mapping (target to source). This is demonstrated by the agreement between the statistical properties of the source images and those of the recovered ones.

1 INTRODUCTION

The upcoming generation of surveys (e.g. SKA) will be able to map neutral hydrogen via HI intensity mapping (Santos et al., 2015). This powerful cosmological probe will help us further our understanding of large scale structure. To extract the relevant information about the matter field from these surveys, we usually resort to summary statistic, such as power spectrum. This is challenging in the non-linear regime due to the contamination of the signal by the baryonic physics, and hence requires higher order statistics. The other approach is to carry out the analysis at the field level, e.g. inference or direct mapping between fields. Previous studies demonstrated the feasibility of building a mapping at the field level between baryons and dark matter (Wadekar et al., 2021; Villanueva-Domingo & Villaescusa-Navarro, 2021; Bernardini et al., 2022). In the light of those existing works, and by utilizing generative adversarial networks (CycleGAN), we aim at building a bijective map between dark matter and two observables, namely neutral hydrogen and magnetic fields magnitude. This is crucial and will pave the way for direct inference of dark matter distribution from maps of observables obtained from different surveys in the near future.

2 METHODS

2.1 DATA

In this study, we use the publicly available CAMELS Multifields Dataset (CMD) (Villaescusa-Navarro et al., 2022) which contains thousands of 2D field maps generated from state-of-the-art hydrodynamics simulations(Villaescusa-Navarro et al., 2021). We consider 256×256 pixels 2D maps, which cover an area of 25×25 $(h^{-1}\mathrm{Mpc})^2$ at $z = 0$, of dark matter (Mcdm), neutral hydrogen (HI) and magnetic fields magnitude (B) from the IllustrisTNG LH set. The choice of the fields in this simple scenario is based on the aim of inferring the matter distribution from observables. In total, each field corresponds to 15000 2D images, each characterized by a set of 6 parameters: matter density (Ω_8), amplitude of matter power spectrum (σ_8), the stellar feedbacks (A_{SN1}, A_{SN1}) and AGN feedbacks (A_{AGN1}, A_{AGN2}).

2.2 MODEL AND TRAINING

To build an invertible mapping between two different fields, we make use of CycleGAN (Zhu et al., 2017), an improvement on "pix2pix" method (Isola et al., 2017) which is trained on paired examples to achieve image-to-image translation. The approach consists of building a function $\mathcal{G} : X \rightarrow Y$ that maps a source field X to a target field Y (forward mapping), simultaneously with another function $\mathcal{F} : Y \rightarrow X$ that translates the target to the source field. To this end, two generators G_X (representing $\mathcal{F}$ and producing the source field images) and G_Y (representing $\mathcal{G}$ and producing the target field images) are trained with two adversarial discriminators D_X and D_Y respectively. Following the prescription in Zhu et al. (2017), there are two main components to the loss function for the training. The adversarial loss – for each of the pair (G_X, D_X) and (G_Y, D_Y) – is given by (Zhu et al., 2017)

$$\mathcal{L}_{\rm GAN}(G_X, D_X, Y, X) = \mathbb{E}_{x\sim p_{\rm data}(x)}[\log D_X(x)] + \mathbb{E}_{y\sim p_{\rm data}(y)}[\log(1 - D_X(G_X(y)))] \quad (1)$$

and

$$\mathcal{L}_{\rm GAN}(G_Y, D_Y, X, Y) = \mathbb{E}_{y\sim p_{\rm data}(y)}[\log D_Y(y)] + \mathbb{E}_{x\sim p_{\rm data}(x)}[\log(1 - D_Y(G_Y(x)))] \quad (2)$$

where $x \sim p_{\rm data}(x)$ and $y \sim p_{\rm data}(y)$ are the data distributions of the source images ($x \in X$) and target images ($y \in Y$) respectively. The consistency loss ensures that the functions $\mathcal{G}$ and $\mathcal{F}$ are inverse of each other such that $G_X(G_Y(x)) \approx x$ and $G_Y(G_X(y)) \approx y$. In other words, an input x (or y) is recovered by applying G_X on $G_Y(x)$ (or applying G_Y on $G_X(y)$). The consistency loss is

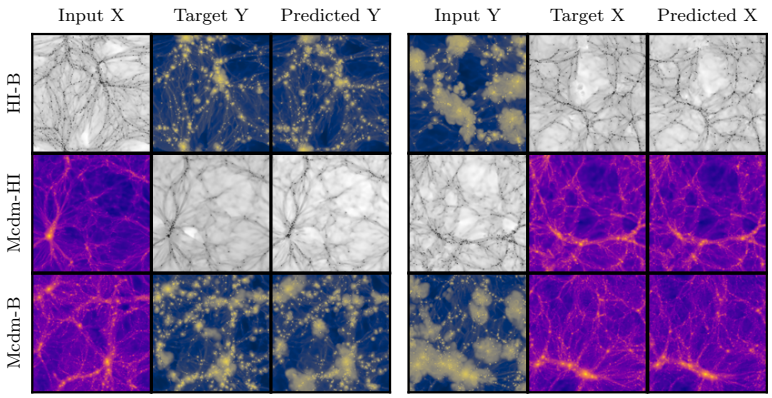

Figure 1: The top, middle, and bottom rows show the results from mapping HI-B, Mcdm-HI, and Mcdm-B respectively. In the first three columns of each row, the first, second and third panels indicate the input to the first generator (for forward mapping), the target and the prediction respectively. In the remaining three columns, the input to the second generator (for inverse mapping), the target and prediction are shown in the 4th, 5th and 6th column respectively. It is worth noting that in a X-Y setting, X and Y designate the source and target fields respectively.

given by (Zhu et al., 2017)

$$\mathcal{L}_{\rm cycle} = \mathbb{E}_{x\sim p_{\rm data}(x)}[||G_X(G_Y(x)) - x||_1] + \mathbb{E}_{y\sim p_{\rm data}(y)}[||G_Y(G_X(y)) - y||_1], \quad (3)$$

where $||.||_1$ denotes the mean absolute error (L1Loss). To further enforce a unique prediction of a given input such that $G_Y(y) \approx y$ and $G_X(x) \approx x$, an identity loss

$$\mathcal{L}_{\rm id} = \mathbb{E}_{y\sim p_{\rm data}(y)}[||G_Y(y) - y||_1] + \mathbb{E}_{x\sim p_{\rm data}(x)}[||G_X(x) - x||_1] \quad (4)$$

is used. The total loss is then given by

$$\mathcal{L}_{\rm tot} = \mathcal{L}_{\rm GAN}(G_X, D_X, Y, X) + \mathcal{L}_{\rm GAN}(G_X, D_X, Y, X) + \lambda_{\rm cycle}\mathcal{L}_{\rm cycle} + \lambda_{\rm id}\mathcal{L}_{\rm id}, \quad (5)$$

where both $\lambda_{\rm cycle}$ and $\lambda_{\rm id}$ are constants that characterize the contributions of the consistency cycle loss and identity loss respectively. Based on the prescription in Zhu et al. (2017), we have that $\lambda_{\rm cycle} = 10$ and $\lambda_{\rm id} = 0.5$ during training.

The generators G_Y and G_X, which have the same architecture, comprise a stage that downsamples the inputs (similar to encoding), 9 residual layers mimicking a bottleneck in variational encoder and finally a stage that upsamples the output from the bottleneck (similar to decoding). The discriminators D_Y and D_X, which are also identical, consist of chaining up 5 convolutional layers where the first three downsample the input by using stride = 2. To have a bit more control on the topology of the generated maps, we condition the input of each component of the model (G_X, D_X, G_Y and D_Y) on the underlying cosmology and astrophysics, i.e the parameters Ω_8, σ_8, $A_{\rm SN1}$, $A_{\rm SN1}$, $A_{\rm AGN1}$ and $A_{\rm AGN2}$. The array of parameters of shape 1×6 is passed through a dense layer with 4096 units whose output is reshaped to 64×64, upsampled to 256×256 via interpolation and finally concatenated along the channel to the input image. The model is trained for 100 epochs with 12000 unpaired examples, i.e. shuffling the set of source images such that they don't match the target images, using Adam optimizer with learning rate of 0.0002. By setting batch size to 1, following Zhu et al. (2017), each epoch takes about 109 minutes on a NVIDIA GeForce GTX 1080 Ti.

3 RESULTS

We present in Figure 1 some predictions by the generators (G_Y and G_X) using input images from test set. Each column in Figure 1 corresponds to the input, target and prediction in a given setup,

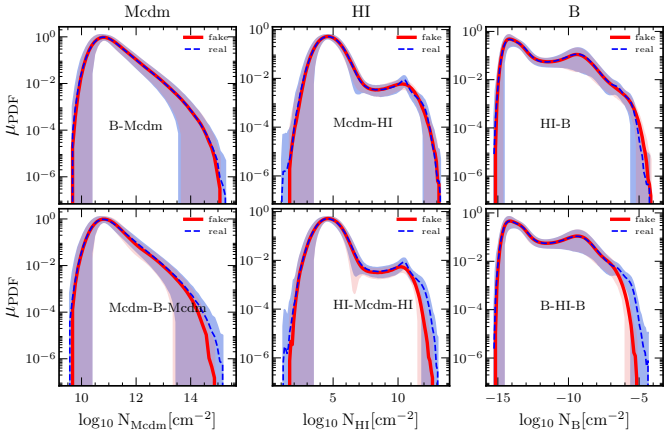

Figure 2: Comparing probability distribution function (PDF) of pixel values of the simulated and generated maps. Results corresponding to each field are shown in each column. Solid red and dashed blue line denote PDFs of fake and real maps respectively. Whereas red and blue shaded area correspond to the standard deviations of the PDFs of fake and real maps respectively. Each column corresponds to PDF of a fields in different setups. The top rows show the comparison between the PDFs of predicted and true maps of a field in each setup. The bottom rows show the consistency check, i.e. assessing if the input is recovered by combining forward and backward mappings.

e.g. HI-B. In the first three columns of each row, we show the result from the forward mapping (generator G_Y representing the function $\mathcal{G}$), i.e. the input is the source field X and the output is the target field Y. The last three columns of each row show the results related to the backward mapping (generator G_X representing the function $\mathcal{F}$), i.e. the input is the target field Y which is translated to the source field X. Visually, the maps output by the generators are in good agreement with the inputs and the quality is comparable to that of the data from IllustrisTNG, overall. However it appears that predicting the magnetic fields B from dark matter or neutral hydrogen seems to be a bit more challenging, as evidenced by the more noticeable difference of the map features between the ground truth and prediction (see 2nd and 3rd columns of both top and bottom rows).
The first metric we use to assess how well the model performs is the probability distribution function (PDF) of pixel intensities. The test set for each setup comprises of 1000 images unseen by the model during training. We then compute the mean $\mu_{\rm PDF}$ and standard deviation $\sigma_{\rm PDF}$ of PDF in the test set of each field in each setup. In Figure 2 we present the PDFs of each field in some setups in each column. The top rows show the results from either forward or backward mappings, whereas the

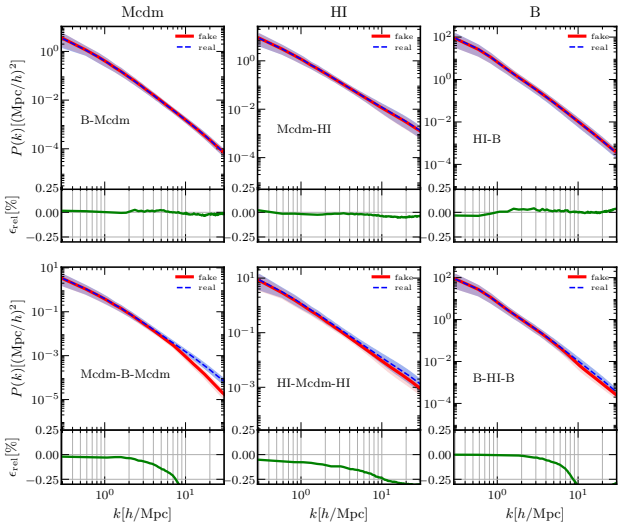

Figure 3: Comparing the resulting power spectra of the simulated and generated maps. Results corresponding to each field are shown in each column. Solid red and dashed blue line denote the averaged power spectum ($P(k)$) of fake and real maps respectively. Whereas red and blue shaded areas correspond to the standard deviations of the $P(k)$ of fake and real maps respectively. The relative error between the two power spectra for each field in each setup is indicated by the solid green line.

results of the consistency test – assessing if an input is recovered by applying forward and backward mappings sequentially – is presented at the bottom row. Results suggest that the model is capable of predicting the source and target fields in each setup using G_X and G_Y respectively, as evidenced by both μ_{PDF} and σ_{PDF} of the data in good agreement with those of the generated maps of each field. We also find that in general the bijective mapping is achieved, i.e. $G_X(G_Y(x)) \approx x$ and $G_Y(G_X(y)) \approx y$, as demonstrated by the μ_{PDF} and σ_{PDF} of the data which agree well with those of the recovered outputs. The relatively small discrepancy at the high end of the distributions can be accounted for by the small number of pixels having those values in the training data, i.e. overdense regions are rare.

The other metric we use to investigate the statistical properties of the images output by our model is the auto-power spectrum $P(k)$. Similar to the results presented in Figure 2, we show the $P(k)$ of the images produced by the forward/backward mapping and the consistency test at the top and bottom rows of Figure 3 respectively. Each panel shows the mean and standard deviation of the $P(k)$ of both real (dashed blue) and fake maps (solid red), and the solid green line at the bottom of each panel shows the relative difference $\left(\frac{P_{\mathrm{fake}}(k)}{P_{\mathrm{real}}(k)} - 1\right)$ between the two $P(k)'$s (fake and real maps). It is clear that the forward and backward mappings are able to produce maps with clustering properties in good agreement with those of the data. Moreover, the mean and variance of $P(k)$ of the recovered maps from the consistency check agree reasonably well with those of the maps from IllustrisTNG, regardless of the increasing difference on larger scales $k > 10\,h/\mathrm{Mpc}$.

4 Conclusion

We have made use of CycleGAN model to build a mapping between fields in IllustrisTNG dataset, allowing us to directly infer the corresponding the target field from a source field. Results show that the predicted maps exhibit statistical properties that agree well with those from the dataset used for training. Moreover, the condition for bijective mapping is met, as demonstrated by the consistency test. By applying the composition function $\mathcal{F} \circ \mathcal{G}(x)$ (or $\mathcal{G} \circ \mathcal{F}(y)$), an input map x (or y) is recovered while the statistics being preserved. This work represents a step froward towards establishing an efficient *direct* mapping between different observables, and hence maximizing the scientific return of future multi-messenger surveys.

REFERENCES

Mauro Bernardini, Robert Feldmann, Daniel Anglés-Alcázar, Mike Boylan-Kolchin, James Bullock, Lucio Mayer, and Joachim Stadel. From ember to fire: predicting high resolution baryon fields from dark matter simulations with deep learning. *Monthly Notices of the Royal Astronomical Society*, 509(1):1323–1341, 2022.

Phillip Isola, Jun-Yan Zhu, Tinghui Zhou, and Alexei A Efros. Image-to-image translation with conditional adversarial networks. In *Proceedings of the IEEE conference on computer vision and pattern recognition*, pp. 1125–1134, 2017.

Mario G Santos, Philip Bull, David Alonso, Stefano Camera, Pedro G Ferreira, Gianni Bernardi, Roy Maartens, Matteo Viel, Francisco Villaescusa-Navarro, Filipe B Abdalla, et al. Cosmology with a ska hi intensity mapping survey. *arXiv:1501.03989*, 2015.

Francisco Villaescusa-Navarro, Daniel Anglés-Alcázar, Shy Genel, David N Spergel, Rachel S Somerville, Romeel Dave, Annalisa Pillepich, Lars Hernquist, Dylan Nelson, Paul Torrey, et al. The camels project: Cosmology and astrophysics with machine-learning simulations. *The Astrophysical Journal*, 915(1):71, 2021.

Francisco Villaescusa-Navarro, Shy Genel, Daniel Angles-Alcazar, Leander Thiele, Romeel Dave, Desika Narayanan, Andrina Nicola, Yin Li, Pablo Villanueva-Domingo, Benjamin Wandelt, et al. The camels multifield data set: Learning the universe's fundamental parameters with artificial intelligence. *The Astrophysical Journal Supplement Series*, 259(2):61, 2022.

Pablo Villanueva-Domingo and Francisco Villaescusa-Navarro. Removing astrophysics in 21 cm maps with neural networks. *The Astrophysical Journal*, 907(1):44, 2021.

Digvijay Wadekar, Francisco Villaescusa-Navarro, Shirley Ho, and Laurence Perreault-Levasseur. Hinet: Generating neutral hydrogen from dark matter with neural networks. *The Astrophysical Journal*, 916(1):42, 2021.

Jun-Yan Zhu, Taesung Park, Phillip Isola, and Alexei A Efros. Unpaired image-to-image translation using cycle-consistent adversarial networks. In *Proceedings of the IEEE international conference on computer vision*, pp. 2223–2232, 2017.